Chemical Engineering Journal 510 (2025) 161860

Contents lists available at ScienceDirect

Chemical Engineering Journal

journal homepage: www.elsevier.com/locate/cej

CO_2 Promoted methanol conversion to methyl formate by photocatalysis

Enqi Chen [a], Xiyi Li [a], Chao Wang [a], Youxun Xu [a], Yang Lan [a], Junwang Tang [a,b,*]

[a] Department of Chemical Engineering, University College London, London WC1E 7JE, UK
[b] Industrial Catalysis Center, Department of Chemical Engineering, Tsinghua University, Beijing 100084, China

ARTICLE INFO

Keywords:
Photocatalysis
CO_2
Methanol
Methyl formate
Bi-metallic

ABSTRACT

Methyl formate (MF), as an important precursor to numerous commercially significant compounds (e.g. dimethyl carbonate, methyl acetate, and ethyl glycol etc), is typically synthesised via the condensation reaction or carbonylation of methanol, requiring relatively high-value precursors (e.g. formic acid or dry CO) while with a low conversion or selectivity. Herein, palladium (Pd) and gold (Au) modified TiO_2 (P25) was designed to use a very low-cost precursor methanol with the assistance of CO_2 to synthesise MF under ambient conditions. Remarkably, a high conversion of methanol (98.1 %) and selectivity to MF (94.9 %) have been achieved under an optimised reaction condition using methanol as the major reactant. In this system, Au significantly enhances charge separation and transfer, and then Pd serves as a final hole acceptor, facilitating the oxidation of methanol to MF by PdAu-modified P25. This synergy boosts the MF formation rate by 15 times compared to single-metal-modified P25 under identical reaction conditions. Further studies reveal that formaldehyde is a pivotal intermediate in the formation of MF and employing CO_2 as a reaction moderator inhibits the methanol over oxidation.

1. Introduction

Methanol has been utilised as a conventional raw material across various sectors including agriculture, pharmaceuticals, energy, and diverse industries[1,2]. In addition, methanol can also serve as an economical C_1 building block for self-coupling to C_2 or multi-carbon chemicals. Methyl formate (MF), notable for its market price being 6 times higher than that of methanol and a global production capacity exceeding 11.25 million metric tonnes annually in 2019[3–6], is crucial in the chemical industry for producing essential chemicals such as formamide, dimethylformamide, and formic acid[6]. In addition, recent study explored the use of MF as a hydrogen carrier, owing to its capacity for hydrogen storage and the thermodynamic favourability of its dehydrogenation compared to other hydrogen carriers[5].

MF is commercially produced through the carbonylation of methanol, catalysed by sodium methoxide while with a low methanol conversion (30 %) under 4.5 MPa and 80℃[7]. Recent advancements have introduced MF via the hydrogenation of CO_2 in the presence of methanol [8–11]. However, these methods often suffer from necessitate relatively high temperatures (200℃)[10]. More importantly, the most commonly reported methods involve aerobic oxidation of methanol through thermal catalysis[12,13]. There is a growing interest in the self-coupling of methanol without using oxygen as a reactant for MF synthesis, as such H_2 instead of H_2O is produced as a valuable byproduct. Although there have been some studies on converting methanol to MF[10,11,14,15] or other value-added chemicals[16–20], these processes either typically operated under harsh conditions (high temperature or pressures), and/or yielded low conversion rates or selectivity (Supplementary Table 1).

Photocatalysis, an emerging green technology, employs photon-induced charge carriers (electrons/holes) to pre-activate stable chemical bonds[21,22]. This process effectively reduces activation barriers and facilitates thermodynamically unfavourable chemical reactions, such as water splitting, CO_2 reduction, and methanol self-coupling, under mild conditions. Although engineering the band structure of photocatalysts by creating heterostructures could modulate the redox potential, accurately manipulating the photocatalyst to prevent the overoxidation of methanol remains challenging. Except the heterostructures, introducing metallic co-catalysts to photocatalysts is a facile strategy to improve the effectiveness of photocatalysis by separating photo-induced charge carriers.

Herein, we report a bi-metallic 0.5Pd1AuP25 photocatalyst for the conversion of methanol to methyl formate under a mild condition. This new photocatalyst achieves a methanol conversion of 98.1 % and an MF selectivity of 94.9 %, together with nearly stoichiometric H_2 synthesis instead of H_2O. This bimetallic photocatalyst outperforms its single-metal counterparts in terms of the production rate and selectivity. The

* Corresponding author.
E-mail address: jwtang@tsinghua.edu.cn (J. Tang).

https://doi.org/10.1016/j.cej.2025.161860
Received 4 November 2024; Received in revised form 5 March 2025; Accepted 20 March 2025
Available online 21 March 2025

inclusion of both Pd and Au on P25 enhances charges separation, offering superior performance. Moreover, by introducing CO_2, the over-oxidation of methanol is mitigated. In addition, formaldehyde (HCHO) is identified as a critical intermediate, influencing both the conversion of methanol and the selectivity towards MF.

2. Results

2.1. Photocatalytic activity

Photocatalysts for MF synthesis were initially selected based on their reliable oxidation/reduction potentials for methanol conversion. As shown in Fig. 1a, only P25 and Nb_2O_5 show activity for MF production together with H_2 and HCHO as the main byproducts, while the selectivity of MF is lower than 10 % in the liquid. The instability of Nb_2O_5, a white powder, is evidenced by its self-reduction to NbO_2, a blue powder [23] (as depicted in Supplementary Fig. 1). Thus, P25, as a mixture of anatase and rutile TiO_2, is selected as the primary photocatalyst for future studies.

Introducing a co-catalyst to the photocatalyst is an effective strategy to improve the photocatalytic activity and tailor the reaction selectivity [24]. In this work, various co-catalysts including Au, Pd, Cu, Ag, Co, and Ru, each at a 1 wt% loading, were incorporated on P25 and tested for methanol conversion (Fig. 1b). The results indicate that all co-catalysts promote the methanol conversion rate, predominantly producing H_2 and HCHO though. Notably, Pd enhances MF production by 29 times from 0.22 μmol to 6.36 μmol and improves selectivity from 5.4 % to 28 % over a 2 h reaction period. Similarly, Au also significantly increases MF yield by approximately 46-fold from 0.22 μmol to 10.96 μmol, with selectivity towards MF reaching 25.8 % among liquid products. Further optimisation of the loading of Pd and Au to P25 was explored to improve the yield and selectivity of MF. (Fig. 1c, Supplementary Fig. 2a-c). Optimal loadings were found to be 1 wt% for Au and 0.5 wt% for Pd on P25. Particularly the bi-metallic co-catalysts exhibits a synergistic effect, leading to significant enhanced catalytic performances. The combination of Au and Pd on P25 (0.1Pd1AuP25) shows a dramatic increase in MF production to 175.2 μmol, which is nearly 900 times higher than P25 only, and also produces 599 μmol of H_2. However, the selectivity of MF is the second highest, being 38 % (Fig. 1c and Supplementary Fig. 2c). The catalyst, 0.5Pd1AuP25, whose real content was analysed by inductively coupled plasma optical emission spectrometer (ICP-EOS) and shown in Supplementary Table 2, presents the highest MF selectivity (45.3 %), which is selected for further improvement. In addition, the catalyst with different loading sequence was also tested but with worse performance (Supplementary Fig. 3).

Subsequent optimization of the reaction conditions included reaction pressures (Supplementary Fig. 4), temperatures (Supplementary Fig. 5), methanol concentrations (Supplementary Fig. 6), and the reaction time (Supplementary Fig. 7). As shown in the Supplementary Fig. 5a, elevated reaction temperature could accelerate the intermediate formaldehyde oxidation reaction to CO, as indicated in Supplementary Fig. 5b. While the formation of MF requires formaldehyde as an important reactant rather than CO. High temperature quickly consumes formaldehyde in the system and simultaneously reduces the formation of MF, leading to a lower MF selectivity. Supplementary Fig. 6a shows that low methanol concentration leads to a high MF selectivity. When methanol concentration is increased, the reaction of methanol oxidation to formaldehyde is facilitated, as presented later in Fig. 5c. Formaldehyde is considered the competing product to MF, so higher methanol concentration generates more formaldehyde, leading to a lower MF selectivity. On the other hand, methanol would be firstly oxidized to formaldehyde, which subsequently reacts with methanol to produce MF

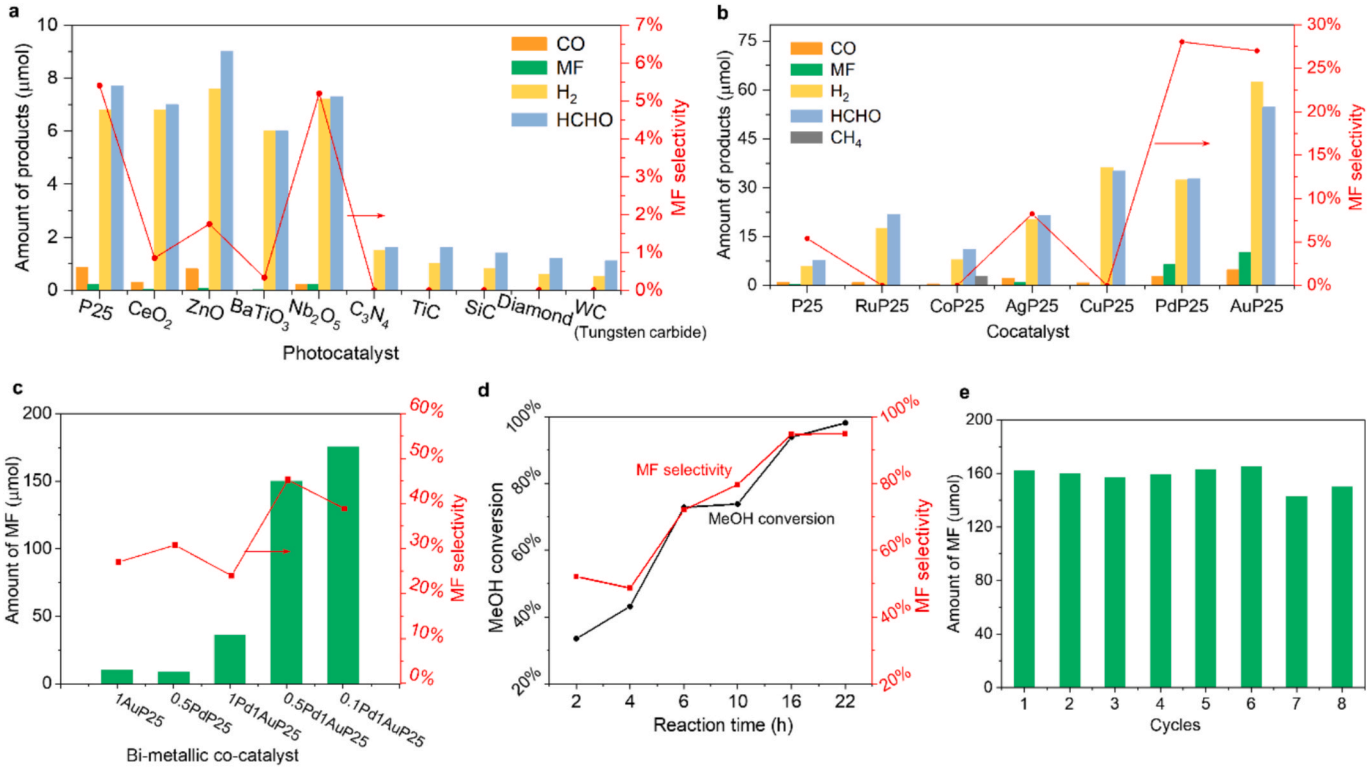

Fig. 1. Catalyst screening for photocatalytic methanol conversion to MF. a Product yield over different photocatalysts. b Product yield over different co-catalyst-modified P25. c Pd and Au bi-metallic co-catalyst performance. d Temporal methanol conversion with increasing selectivity over 0.5Pd1AuP25 under optimised reaction condition (Optimised reaction conditions: 10 mg catalyst was dispersed into 40 mL of 0.025 % methanol in acetonitrile and purged with CO_2 for 30 min. The system was irradiated by using a 365 nm LED light source at room temperature under the pressure of 6 bar). e Stability test using 0.5Pd1AuP25 catalyst for a 4 h run in each cycle.

when the concentration of methanol is moderate, which is also indicated later in Fig. 5. So an appropriate methanol concentration is important for the selective MF production. Thus, higher temperatures and methanol concentrations can decrease MF selectivity, while extending the reaction time results in enhanced MF selectivity. Consequently, optimised conditions are a 0.025 % methanol in acetonitrile operating at room temperature for a prolonged reaction (Fig. 1d). Under these conditions, MF selectivity peaks at 94.9 % and remains stable even after 16 h, indicating an equilibrium between MF and HCHO in the liquid, and the methanol conversion progressively increases to 98.1 %. Stability test of the optimized condition, as shown in Fig. 1e, shows consistent MF yield over eight 4-h cycles, confirming the high stability of the catalyst during the photocatalytic methanol conversion reaction.

2.2. Photocatalysts characterization

Raman spectra were initially employed to investigate the structure of the catalysts (Fig. 2a), where all samples exhibited characteristic Raman peaks of the P25 anatase phase, at 144 cm^{-1}(E_g), 198 cm^{-1}(E_g), 399 cm^{-1}(B_{1g}), 512 cm^{-1}(A_{1g}), and 639 cm^{-1}(E_g), respectively. These results confirm the stable framework of anatase TiO_2 after cocatalyst loading. Additionally, powder X-ray diffraction (PXRD) analysis of pristine P25 and 0.5Pd1AuP25 presented in Supplementary Fig. 8, shows peaks indicative of the anatase phase of TiO_2 (JCPDS NO. 84–1286) without detectable Pd and Au peaks. In addition, the catalyst of 0.5Pd1AuP25 before and after reaction shows the same XRD result. Combined with the stability test results in Fig. 1e, it underscores the robustness of 0.5Pd1AuP25 as a photocatalyst for methanol conversion.

Photoluminescence (PL) spectroscopy, as shown in Fig. 2b, was used to investigate the charge separation and recombination process of the photocatalysts. P25 shows the highest PL emission, implying an intense charge recombination process. Conversely, the addition of Pd and Au causes a reduction in the PL intensity, with the lowest signals observed in Pd and Au co-modified P25, suggesting enhanced charge transfer to Pd and/or Au instead of local recombination within P25. Ultraviolet–visible diffuse reflectance spectroscopy (UV–Vis DRS) was utilised to assess the photon absorption properties (Supplementary Fig. 9). The absorption profile (both absorption edge and peak) of all samples remains almost the same, indicating that P25 harvests light for photon-induced carrier generation. A slightly enhanced light absorption at the visible light region after the introduction of co-catalyst is observed, probably due to the interband absorption and/or scattering by these particles[25]. Au modified catalyst shows the characteristic peak around 550 nm due to the plasmonic effect. The photoelectric properties of P25 and metal modified P25 were studied by transient photocurrent responses and electrochemical impedance spectroscopy (EIS) as shown in Supplementary Fig. 10. The photocurrent of bi-metallic PdAuP25 is much higher than that of mono-metallic modified P25 and bare P25, indicating that the bi-metallic PdAu cocatalyst shows the highest photocurrent, which would facilitate methanol oxidation. The electrochemical impedance spectra also suggest that PdAuP25 has the smallest resistance.[26,27].

The morphology and dispersity of the Pd and Au cocatalysts were examined using high-angle annular dark-field scanning transmission electron microscopy (HAADF-STEM). As shown in Fig. 2c, P25 supports are clearly shown with the size of about 30 nm. Bright dots are also observed to uniformly disperse on the P25 supports. Detailed examination of one bright dot (blue rectangle in Fig. 2c) reveals the fine structure of the co-catalyst with a size of 2 nm (Fig. 2d). And its lattice fringes are observed with a lattice constant of 0.238 nm (Supplementary Fig. 11) corresponding to the Au nanoparticle. Energy Dispersive X-Ray Analysis (EDX) was applied to obtain compositional information of the nanoparticles (Fig. 2e). Both Au and Pd elements are detected, suggesting the formation of Au nanoparticles on the surface of P25 with smaller, indistinct Pd clusters on Au nanoparticles. Furthermore, the used PdAuP25 catalyst was also characterised by HRTEM and EDX as shown in Supplementary Fig. 12 and Supplementary Fig. 8, indicating a high stability of the catalyst.

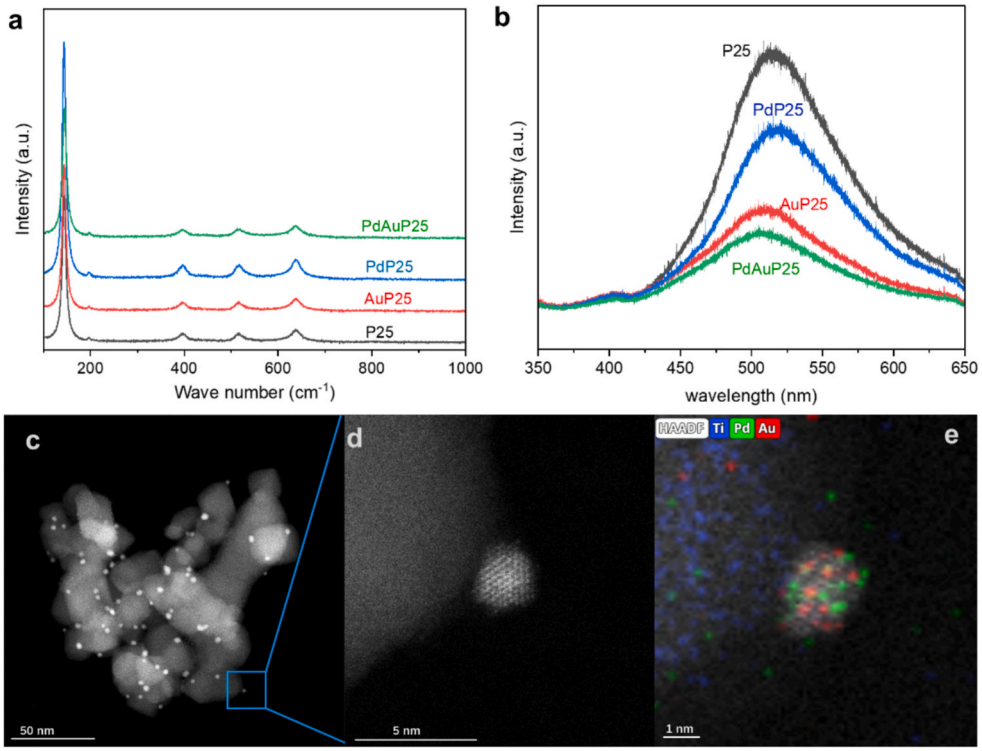

Fig. 2. Characterisation of the photocatalysts. a Raman spectrum of P25, 1AuP25, 1PdP25, and 0.5Pd1AuP25. b Photoluminescence (PL) of P25, 1AuP25, 1PdP25, and 0.5Pd1AuP25. c STEM image of 0.5Pd1AuP25. d STEM image of the blue rectangle in c. e EDX elements mapping of 0.5Pd1AuP25.

2.3. Charge transfer process

The charge transfer process of the optimised photocatalyst (0.5Pd1AuP25) was investigated by in-situ X-ray photoelectron spectroscopy (XPS) under light irradiation. The in-situ XPS spectra of AuP25 and PdP25 were firstly investigated as shown in Fig. 3a and 3b. A 0.2 eV positive shift of Pd^{2+} 3*d* peak is detected under the light irradiation (red line) compared to the dark condition (black line). This shift indicates that Pd works as a hole accepter which agrees with the previous report [28]. For AuP25, the in-situ XPS (Fig. 3b) result shows a 0.1 eV positive shift for Au 4*f* peak, confirming that Au works as the hole acceptor under the light irradiation[29]. Further in-situ XPS spectra of the 0.5Pd1AuP25 results (Fig. 3c and d) show a more pronounced positive shift of 0.4 eV in the Pd^{2+} 3*d* peak under light irradiation, whereas the Au 4*f* peak displays identical binding energy both in dark and under light irradiation. Taking into account the morphology of 0.5Pd1AuP25 shown in Fig. 2e, the synthetic process outlined in the Methods section, and the charge transfer process of single-metal-modified P25 discussed above, this phenomenon suggests that the Au–Pd bimetallic configuration acts as an effective hole acceptor and very likely the photo-induced holes transferred from P25 to Pd species via Au[30,31]. The charge transfer discussed by band theory shows the same result shown in Supplementary Fig. 13.

2.4. Reaction mechanism

Isotope labelling experiments were carried out to provide deep insights into the reaction mechanism by tracking the carbon source involved. When methanol labelled with ^{13}C ($^{13}CH_3OH$) was combined with normal CO_2, the primary product MF displays a main mass spectrometric (MS) peak at $m/z = 62$, indicating that both carbon atoms in MF originated from methanol (Fig. 4 a1). A secondary, smaller peak at $m/z = 61$ suggests the product MF with one carbon atom from labelled methanol and the other from normal CO_2. Concurrently, experiments using $^{13}CO_2$ to react with normal CH_3OH under identical reaction conditions (Fig. 4b1), indicates the same result that the formation of MF is predominant by methanol conversion and a small portion is from the reaction between CO_2 and CH_3OH. Further analysis identifies formaldehyde (HCHO) as a critical intermediate in the reaction. When $^{13}CH_3OH$ was used with normal CO_2, the peak for HCHO appeared at $m/z = 31$ (Fig. 4 a2). While, when $^{13}CO_2$ with normal methanol was used, the produced HCHO showed a peak at $m/z = 30$ (Fig. 4 b2). The MS result indicates that HCHO primarily originates from methanol oxidation rather than CO_2 reduction. In addition, the source of carbon in the product CO was similarly traced using $^{13}CH_3OH$ and $^{13}CO_2$ individually and the results suggest that CO is mainly from methanol. These experiments clarify methanol as the primary reactant, which is converted into MF, HCHO, and CO, while only a minimal amount of CO_2 takes part in the reaction for the production of MF and CO. Additional tests were conducted to investigate the overoxidation of methanol to CO_2 using

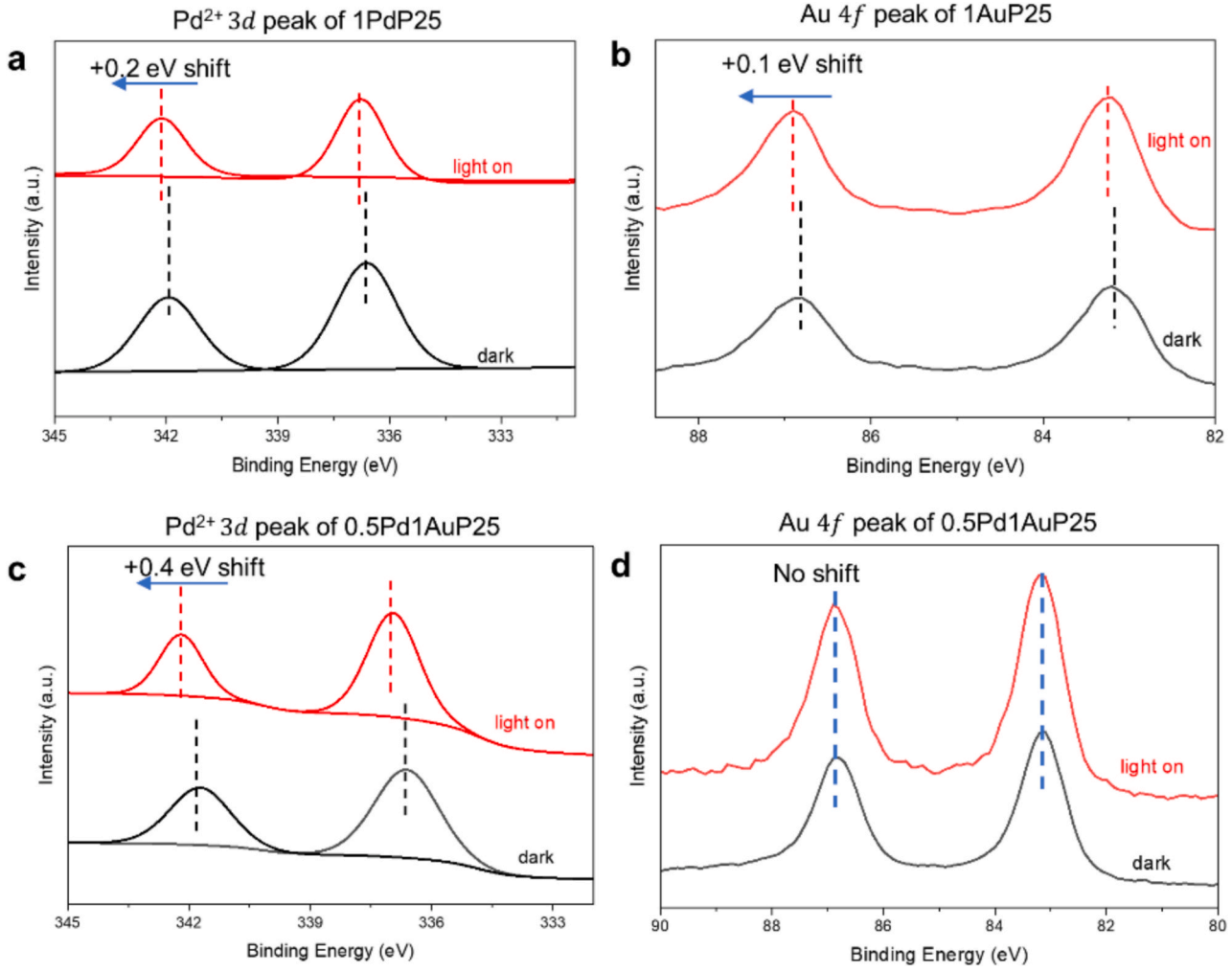

Fig. 3. In-situ XPS results under dark and light irradiation condition for Pd^{2+} *3d* of PdP25 (a), Au^0 *4f* of AuP25 (b), Pd^{2+} *3d* of PdAuP25 (c), and Au^0 *4f* of PdAuP25 (d).

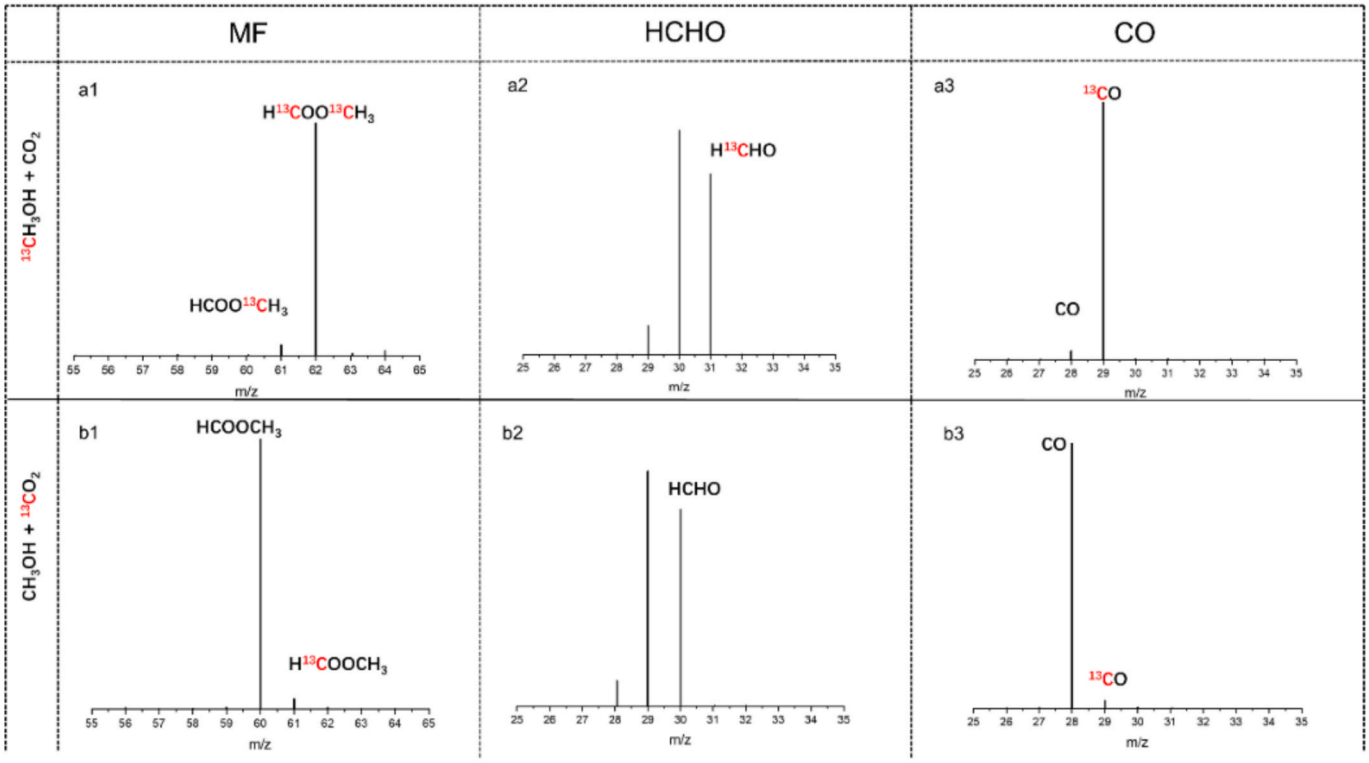

Fig. 4. Mass spectra of isotope labelling experiments over 0.5Pd1AuP25. a1 – a3 Mass spectra of products using ^{13}C methanol and normal CO_2 as reactants. b1 – b3 Mass spectra of products using $^{13}CO_2$ and normal methanol as reactants.

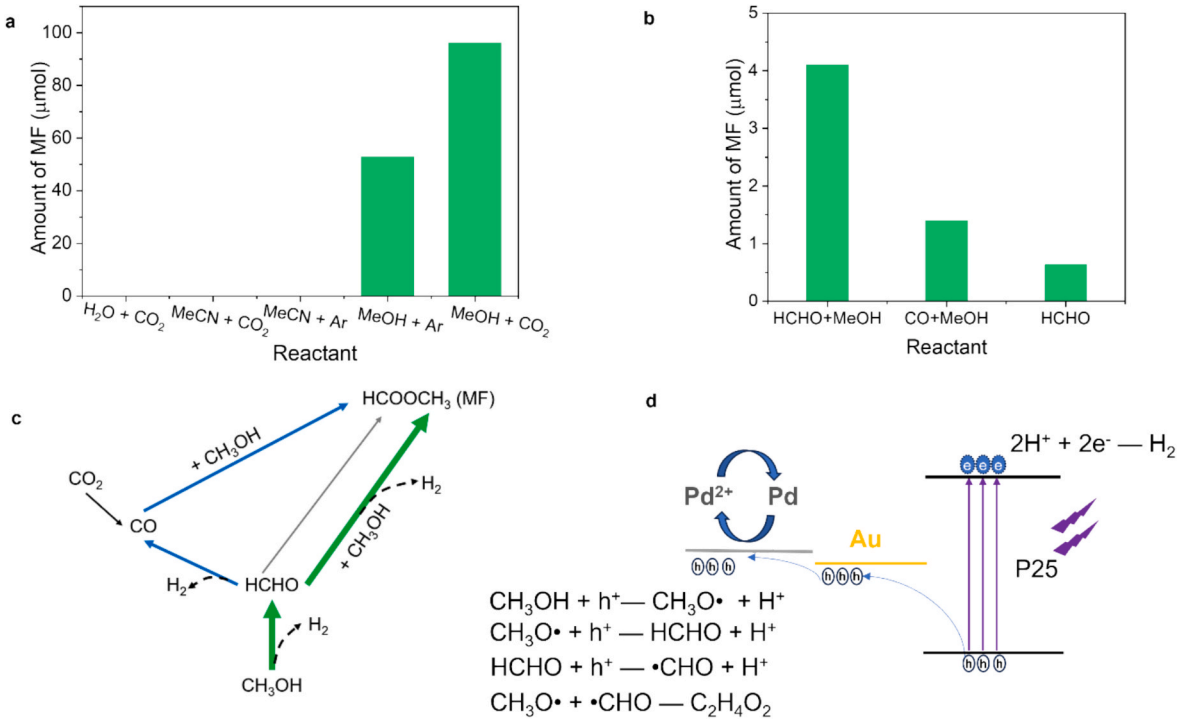

Fig. 5. Reaction mechanistic study. a Control experiments for studying the source of MF and the function of CO_2. b Product yield using possible intermediates (CO and HCHO). c reaction pathways of methanol conversion where green arrow shows the main pathway of MF formation; blue arrow shows the secondary pathway; grey arrow shows the minor pathway; black arrow shows the influence of CO_2 in the system. d Schematic of charge transfer and reaction pathways.

either $^{13}CH_3OH$ and CO_2 or CH_3OH and $^{13}CO_2$ as reactants (Supplementary Fig. 14). The results show that all CO_2 almost come from the feed gas, rather than the oxidation of methanol.

Control experiments further highlighted the role of CO_2 in the reaction system. As shown in the control experiments (Supplementary Fig. 15), group (1) shows that CO_2 could be reduced to CO under the

optimised condition by 0.5Pd1AuP25. This result, together with the isotopic experiments proves that CO_2 could be a precursor to form MF through CO. Group (2) and (3) do not produce any products, indicating that nothing could be produced without methanol as a reactant under the present condition. Fig. 5a explores the influence of CO_2 on MF production, which shows that the amount of MF increases when replacing Ar with CO_2 in the system, demonstrating that CO_2 has a positive impact on converting methanol to MF. To this end, it is concluded that CO_2 in the system not only participates directly in the reactions but also plays a crucial role in inhibiting the overoxidation of methanol, which is discussed in Supplementary Fig. 16.

To further analyse the reaction pathway, different feedstocks (HCHO + MeOH, CO + MeOH, and HCHO alone) were tested for MF production (Fig. 5b and Supplementary Fig. 17). When sufficient methanol is present in the reaction (Fig. 1), HCHO emerges as a major product in the liquid phase. Therefore, HCHO was added as one feedstock to react with methanol, which shows the highest production of MF in the control experiment (Fig. 5b and Fig. 5c green pathway). In parallel, experiments where HCHO was replaced by CO for MF formation under identical reaction conditions were also conducted (Fig. 5b and Fig. 5c blue pathway). Although CO is often reported as an active intermediate in various reactions, it results in a lower MF in this system. Additionally, employing HCHO as the only reactant (Fig. 5b and Fig. 5c grey pathway) shows the lowest MF production, indicating that the formation of MF does not solely depend on the self-coupling of HCHO. These observations suggest that the primary pathway for the photocatalytic formation of MF likely involves the coupling of HCHO and MeOH (green pathway). Additionally, a secondary pathway also appears plausible, which involves the coupling of MeOH and CO, which is presumably derived from the reduction of CO_2 (blue pathway).

Based on the above discussion, the proposed reaction mechanism for photocatalytic methanol conversion of methanol to MF over 0.5Pd1AuP25 is depicted in Fig. 5d and Supplementary Fig. 13. When the incident light irradiates P25, electrons in valence band (VB) of P25 would be excited to its conduction band (CB). Meanwhile, the holes migrate from the VB of P25 to Au particles and subsequently to Pd species. This transfer leads to the formation of Pd^{2+} ions, leaving Au to neutral. The Pd^{2+} ions act as the active site where methanol can be oxidised to the methoxy group and a proton (Eq. (1)[32–36]. Then, the adsorbed methoxy intermediate is oxidised to formaldehyde and a proton (Eq. (2). Subsequently, the formaldehyde is further oxidised into a formyl (•CHO) (Eq. (3). Finally, the coupling of methoxy and formyl leads to the formation of MF (Eq. (4). Concurrently, the protons are reduced by photoelectrons to produce H_2 on P25. The surface adsorption and possible reaction mechanism are also discussed as shown in Supplementary Fig. 18 and Supplementary Fig. 19.

$$CH_3OH + h^+ - CH_3O\bullet + h^+ \quad (1)$$

$$CH_3O\bullet + h^+ - HCHO + H^+ \quad (2)$$

$$HCHO + h^+ - \bullet CHO + H^+ \quad (3)$$

$$CH_3O\bullet + \bullet CHO - C_2H_4O_2 \quad (4)$$

3. Discussion

In summary, PdAu-decorated P25 has shown the high efficiency and stability as a photocatalyst for the anaerobic methanol conversion to methyl formate in a batch reactor under ambient conditions. Remarkably, a 98.1 % conversion of methanol is achieved, with a selectivity for MF of 94.9 %. In the meantime, H_2 instead of water is obtained as the main reduction product. Extensive structural characterisations, along with spectroscopic measurements, and mechanism analysis, reveal that the bimetallic PdAu cocatalyst can improve the activity more than 15 times compared with individual cocatalyst, which is due to a synergistic effect between Au and Pd. This is primarily because the Au nanoparticles facilitate the efficient transfer of holes from P25 to the Pd cluster, significantly boosting the activity for MF formation. Furthermore, isotopic labelling experiments and control reactions suggest that CO_2 suppresses the overoxidation of methanol, leading to efficient utilisation of reactants. Additionally, CO_2 shows a minor contribution to the formation of MF by reducing CO_2 to CO, which is also a reactant in MF formation. This results in the high selectivity for MF production.

4. Methods

4.1. Photocatalysts synthesis

The single metal (Ru, Co, Ag, Cu, Pd, Au) modified P25 was synthesised using $NaBH_4$ (Sigma Aldrich, ≥ 96 %) reduction method. First, 200 mg P25 was dispersed into 200 mL deionised water under stirring. Then, taking Au as an example, different amounts of gold (III) chloride trihydrate (Sigma Aldrich, 99.9 %) aqueous solution (2 mg_{Au}/mL) were added to the P25 dispersions and stirred for 2 h. After that, a certain amount of fresh $NaBH_4$ (0.1 M) with a mole ratio of 5 ($NaBH_4$/Au) was added to the mixture and stirred for another 1 h. The photocatalyst was obtained by centrifugation, washed with deionised water for three times, and dried in a vacuum oven for 12 h at 80 °C. The photocatalyst synthesized by this method was denoted as AuP25 (the name indicates 1 wt% Au modified P25).

For synthesis of 0.5Pd1AuP25 (the name indicates 0.5 wt% Pd and 1 wt% Au modified P25), 200 mg AuP25 prepared above was dispersed into 200 ml deionised water under stirring. Then, 1 mL of $PdCl_2$ (Aldrich, 99.999 %) aqueous solution (1 mg_{Pd}/mL) was added to the solution for a 2-hour stirring. After that, a certain amount of $NaBH_4$ (0.1 M) with a mole ratio of 5 ($NaBH_4$/Pd) was added to the mixture and stirred for another 1 h. The photocatalyst was obtained by centrifugation, washed with deionised water for three times, and dried in the vacuum oven for 12 h at 80 °C. The photocatalyst synthesized was denoted as 0.5Pd1AuP25.

4.2. Characterisation

The powder X-ray (XRD) spectra were measured with a Rigaku SmartLab SE using a Cu Kα1 source (60 kV, 60 mA). Raman spectroscopy was performed at Horiba LabRAM HR Evolution with a 532 nm laser. Ultraviolet–visible diffuse reflectance spectroscopy (UV–Vis DRS) was recorded by an Agilent Cary 5000 in reflectance mode using standard $BaSO_4$ powder as a reference. The chemical environment was evaluated using X-ray photoelectron spectroscopy (XPS) with an Axis Supra (Kratos Analytical Ltd., UK) system equipped with an Al Kα X-ray source (1486.6 eV) operating at 200 W for survey scans and 300 W for core level spectra. The binding energy was calibrated by the C 1 *s* peak at 284.8 eV. In-situ XPS experiment was conducted using the same XPS machine mentioned above by equipping a 365 LED light source. PL spectroscopy was collected by Horiba LabRAM HR Evolution with a 325 nm excitation laser. STEM imaging was conducted using Cs-corrected scanning transmission electron microscope (FEI Titan Cubed Themis G2 300) operated at 300 kV with a dwell time of 10 μs. The elemental mapping was obtained by energy-dispersive spectroscopy (EDS) in the same Cs-corrected scanning transmission electron microscope (FEI Titan Cubed Themis G2 300) with a dwell time of 20 μs. In-situ diffuse reflectance infrared Fourier transform spectroscopy (DRIFTS) experiments were performed on a FTIR spectrometer (Thermo Nicolet iS50, with Harrick Diffuse Reflectance). Agilent-5110 inductively coupled plasma optical emission spectrometer was used for element content measurement.

4.3. Photocatalytic methanol conversion

The photocatalytic methanol conversion was conducted in a batch

reactor (150 mL with a quartz window on the top, and a thermal couple inside the reactor). A 365 nm LED light (Beijing Perfect Light, PLS-LED 100) was used as the light source. In the catalyst screening experiment and stability test, 20 mg of sample was dispersed in 40 mL of 0.25 % methanol (Supra Solv Methanol for GCMS, Sigma) in acetonitrile (Sinopharm), and the mixture was allowed to sonicate for 15 min to achieve a good dispersion. Afterward, CO_2 (Air Liquide, 99.999 %) was used to purge the system for 30 min to remove the oxygen in the batch reactor, and to increase the CO_2 pressure to 6 bar. Then, the 365 nm LED (80 W) irradiated from the top quartz window of the reactor for two hours at room temperature. During the reaction, the mixture was continuously stirred to facilitate the mass transfer. After the reaction, gas phase products were firstly analysed by GC (Shimadzu GC-2023, equipped with Barrier Discharge Ionization Detector, through the 5A collum). For liquid products, the photocatalyst was separated by filtration first, and the solution was analysed using GC (Shimadzu GC-2023, equipped with Barrier Discharge Ionization Detector, through the DB-WAX collum). All products in the reaction mixture were quantified with an external calibration method. Under the optimised reaction condition (Fig. 1d), 10 mg 0.5Pd1AuP25 was dispersed into a 40 mL mixture (10 μL methanol and 40 mL acetonitrile). Then, CO_2 was used to purge the system for 30 min following with a two-hour 365 nm LED (80 W) irradiation. The reaction conditions for the control experiments (Supplementary Fig. 15) were conducted under the same condition of the screening experiments but different for the solvents, where pure water, pure acetonitrile and pure methanol were used. In the stability test, the used photocatalyst was filtered and then washed for the next cycle of the stability test.

4.4. Isotope labelling experiment

For the isotope labelling experiment, a similar photocatalytic process was conducted except $^{13}CH_3OH$ (^{13}C enrichment > 99 % atom, Shanghai Institute of Chemical Engineering) or $^{13}CO_2$ (^{13}C enrichment > 99 % atom, Shanghai Institute of Chemical Engineering) was used as the feed gas. Typically, 20 mg 0.5Pd1AuP25 photocatalyst was used in the batch reactor. For the labelled methanol experiment, the feedstocks were 50 μL $^{13}CH_3OH$ in 40 mL MeCN and 1 bar CO_2. On the contrary, for the labelled CO_2 experiment, the feed stocks were 50 μL CH_3OH in 40 mL MeCN and 1 bar $^{13}CO_2$. All were introduced under a 100 W LED with 365 nm light source for 3 h. The products containing C-isotope were analysed by GCMS-QP2020 NX (Shimadzu).

4.5. Calculation of MF selectivity

The selectivity of MF was calculated based on the measured liquid products, which include formaldehyde and methyl formate. The selectivity was calculated using the following equation:

$$MFselectivity = \frac{2 \times n_{MF}}{2 \times n_{MF} + n_{HCHO}} \times 100\%$$

where n is the yield of products.

4.6. Calculation of methanol conversion

The conversion of methanol was calculated depending on the initial amount of methanol (n_i) and the amount of methanol after the reaction (n_f).

$$MethanolConversion = \frac{n_i - n_f}{n_i} \times 100\%$$

Here n_i was the amount of methanol after CO_2 purging for 30 min, as some loss occured during purging. For the condition with the best methanol conversion, the amount of methanol added into the reactor was 10 μL (equivalent to 247 μmol). After a 30-min purge, the amount decreased to 147 μmol, which was n_i in the system.

CRediT authorship contribution statement

Enqi Chen: Writing – review & editing, Writing – original draft, Methodology, Investigation, Formal analysis, Data curation. **Xiyi Li:** Writing – review & editing, Methodology, Investigation. **Chao Wang:** Writing – review & editing, Investigation. **Youxun Xu:** Writing – review & editing, Investigation. **Yang Lan:** Writing – review & editing, Supervision. **Junwang Tang:** Writing – review & editing, Supervision, Funding acquisition, Conceptualization.

Declaration of competing interest

The authors declare that they have no known competing financial interests or personal relationships that could have appeared to influence the work reported in this paper.

Acknowledgements

J. T. acknowledges the financial support from the National Key R&D Program of China (2024YFF0506201), NSFC projects (Grant No: U23B20162 and 22250710677) and Beijing Municipal Project (C2022007). All authors also thank UK EPSRC (EP/ S018204/2). Y. L. and X. L. acknowledge the funding from the UK Research and Innovation (UKRI) (Reference No.: 10045035) under the UK government's Horizon Europe funding guarantee grant number (GH2 101070721). We are grateful for the in-situ XPS characterization by Dr. Kaiqi Nie from Industry Catalysis Centre, Tsinghua University. We are also thankful to the STEM characterization by Hairong Jiang from the department of chemical engineering in Tsinghua University.

Author contributions

J.T. designed and supervised the progress of the whole project. E.C. designed and conducted experiments and analysed data. X.L and C.W. assisted with the conduction of the activity test. Y.X. and Y.L. contributed to the discussion of the photocatalytic mechanism. All authors co-drafted the manuscript and approved the final version of the manuscript.

Appendix A. Supplementary data

Supplementary data to this article can be found online at https://doi.org/10.1016/j.cej.2025.161860.

Data availability

Data will be made available on request.

References

[1] F. Dalena, A. Senatore, A. Marino, A. Gordano, M. Basile, A. Basile, Methanol Production and Applications: An Overview, in: Methanol: Science and Engineering, Elsevier, 2018: pp. 3–28. https://doi.org/10.1016/B978-0-444-63903-5.00001-7.
[2] H. Wang, H. Qi, X. Sun, S. Jia, X. Li, T.J. Miao, L. Xiong, S. Wang, X. Zhang, X. Liu, A. Wang, T. Zhang, W. Huang, J. Tang, High quantum efficiency of hydrogen production from methanol aqueous solution with PtCu–TiO2 photocatalysts, Nat. Mater. 22 (2023) 619–626, https://doi.org/10.1038/s41563-023-01519-y.
[3] L. Rong, Z. Xu, J. Sun, G. Guo, New methyl formate synthesis method: Coal to methyl formate, J. Energy. Chem. 27 (2018) 238–242, https://doi.org/10.1016/j.jechem.2017.07.015.
[4] D. Kaiser, L. Beckmann, J. Walter, M. Bertau, Conversion of green methanol to methyl formate, Catalysts 11 (2021), https://doi.org/10.3390/catal11070869.
[5] R. Sang, Z. Wei, Y. Hu, E. Alberico, D. Wei, X. Tian, P. Ryabchuk, A. Spannenberg, R. Razzaq, R. Jackstell, J. Massa, P. Sponholz, H. Jiao, H. Junge, M. Beller, Methyl formate as a hydrogen energy carrier, Nat. Catal 6 (2023) 543–550, https://doi.org/10.1038/s41929-023-00959-8.
[6] Q. Shi, X. Wei, A. Raza, G. Li, Recent Advances in Aerobic Photo-Oxidation of Methanol to Valuable Chemicals, ChemCatChem 13 (2021) 3381–3395, https://doi.org/10.1002/cctc.202100104.

[7] W. Reutemann, H. Kieczka, Formic Acid, Ullmann's Encyclopedia of Industrial Chemistry, Wiley-VCH, Weinheim (2002), https://doi.org/10.1002/14356007.a12.
[8] B.G. Schieweck, N.F. Westhues, J. Klankermayer, A highly active non-precious transition metal catalyst for the hydrogenation of carbon dioxide to formates, Chem. Sci 10 (2019) 6519–6523, https://doi.org/10.1039/c8sc05230a.
[9] J. Chen, S. Qin, G. Song, T. Xiang, F. Xin, X. Yin, Shape-controlled solvothermal synthesis of Bi2S3 for photocatalytic reduction of CO2 to methyl formate in methanol, Dalton. Trans. 42 (2013) 15133–15138, https://doi.org/10.1039/c3dt51887f.
[10] C. Wu, Z. Zhang, Q. Zhu, H. Han, Y. Yang, B. Han, Highly efficient hydrogenation of carbon dioxide to methyl formate over supported gold catalysts, Green. Chem. 17 (2015) 1467–1472, https://doi.org/10.1039/c4gc01818d.
[11] J.J. Corral-Pérez, A. Bansode, C.S. Praveen, A. Kokalj, H. Reymond, A. Comas-Vives, J. Vandevondele, C. Copéret, P.R. Von Rohr, A. Urakawa, Decisive role of perimeter sites in silica-supported Ag nanoparticles in selective hydrogenation of CO2 to methyl formate in the presence of methanol, J. Am. Chem. Soc 140 (2018) 13884–13891, https://doi.org/10.1021/jacs.8b08505.
[12] G.T. Whiting, S.A. Kondrat, C. Hammond, N. Dimitratos, Q. He, D.J. Morgan, N. F. Dummer, J.K. Bartley, C.J. Kiely, S.H. Taylor, G.J. Hutchings, Methyl formate formation from methanol oxidation using supported gold-palladium nanoparticles, ACS. Catal 5 (2015) 637–644, https://doi.org/10.1021/cs501728r.
[13] D.H. Wang, K.M. Engle, B.F. Shi, J.Q. Yu, Ligand-enabled reactivity and selectivity in a synthetically versatile Aryl C-H olefination, Science 327 (2010) (1979) 315–319, https://doi.org/10.1126/science:1182512.
[14] B. Wang, S. Zhong, S. Tang, H. Yue, K. Ma, C. Liu, B. Liang, Photocatalytic Production of Methyl Formate by Methanol Self-Coupling: From Oxidative Dehydrogenation to Direct Dehydrogenation, Ind. Eng. Chem. Res 60 (2021) 9684–9695, https://doi.org/10.1021/acs.iecr.1c01369.
[15] S. Qin, F. Xin, Y. Liu, X. Yin, W. Ma, Photocatalytic reduction of CO2 in methanol to methyl formate over CuO-TiO2 composite catalysts, J. Colloid. Interface. Sci 356 (2011) 257–261, https://doi.org/10.1016/j.jcis.2010.12.034.
[16] K.M. Lee, J.H. Jang, M. Balamurugan, J.E. Kim, Y.I. Jo, K.T. Nam, Redox-neutral electrochemical conversion of CO2 to dimethyl carbonate, Nat. Energy 6 (2021) 733–741, https://doi.org/10.1038/s41560-021-00862-1.
[17] Y. Chen, H. Wang, Z. Qin, S. Tian, Z. Ye, L. Ye, H. Abroshan, G. Li, Ti: XCe1-xO2 nanocomposites: A monolithic catalyst for the direct conversion of carbon dioxide and methanol to dimethyl carbonate, Green. Chem. 21 (2019) 4642–4649, https://doi.org/10.1039/c9gc00811j.
[18] Y. Chen, Y. Li, W. Chen, W.W. Xu, Z. Kang Han, A. Waheed, Z. Ye, G. Li, A. Baiker, Continuous dimethyl carbonate synthesis from CO2 and methanol over BixCe1−xOδ monoliths: effect of bismuth doping on population of oxygen vacancies, activity, and reaction pathway, Nano. Res. 15 (2022) 1366–1374, https://doi.org/10.1007/s12274-021-3669-4.
[19] X. Wei, Y. Li, L. Chen, J. Shi, Formic Acid Electro-Synthesis by Concurrent Cathodic CO2 Reduction and Anodic CH3OH Oxidation, Angewandte. Chemie. -. International. Edition 60 (2021) 3148–3155, https://doi.org/10.1002/anie.202012066.
[20] S. Jin, W. Shao, S. Chen, L. Li, S. Shang, Y. Zhao, X. Zhang, Y. Xie, Ultrathin In-Plane Heterostructures for Efficient CO2 Chemical Fixation, Angewandte. Chemie. -. International. Edition 61 (2022), https://doi.org/10.1002/anie.202113411.
[21] X. Li, C. Wang, J. Tang, Methane transformation by photocatalysis, Nat. Rev. Mater 7 (2022) 617–632, https://doi.org/10.1038/s41578-022-00422-3.
[22] S.J.A. Moniz, S.A. Shevlin, D.J. Martin, Z.X. Guo, J. Tang, Visible-light driven heterojunction photocatalysts for water splitting-a critical review, Energy, Environ. Sci 8 (2015) 731–759, https://doi.org/10.1039/c4ee03271c.
[23] C.K. Gupta, A.K. Suri, Extractive Metallurgy of Niobium, first ed., CRC, 1994.
[24] X. Li, J. Yu, M. Jaroniec, X. Chen, Cocatalysts for selective photoreduction of CO 2 into solar fuels, Chem. Rev 119 (2019) 3962–4179, https://doi.org/10.1021/acs.chemrev.8b00400.
[25] S. Sorcar, Y. Hwang, J. Lee, H. Kim, K.M. Grimes, C.A. Grimes, J.-W. Jung, C.-H. Cho, T. Majima, M.R. Hoffmann, S.-I. In, CO_2, water, and sunlight to hydrocarbon fuels: a sustained sunlight to fuel (Joule-to-Joule) photoconversion efficiency of 1%, Energy, Environ. Sci 12 (2019) 2685–2696, https://doi.org/10.1039/C9EE00734B.
[26] C. Cheng, H. Xu, M. Ni, C. Guo, Y. Zhao, Y. Hu, Interfacial electron interactions governed photoactivity and selectivity evolution of carbon dioxide photoreduction with spinel cobalt oxide based hollow hetero-nanocubes, Appl. Catal. B 345 (2024) 123705, https://doi.org/10.1016/j.apcatb.2024.123705.
[27] X. Lin, S. Xia, L. Zhang, Y. Zhang, S. Sun, Y. Chen, S. Chen, B. Ding, J. Yu, J. Yan, Fabrication of Flexible Mesoporous Black Nb $_2$ O $_5$ Nanofiber Films for Visible-Light-Driven Photocatalytic CO $_2$ Reduction into CH $_4$, Adv. Mater. 34 (2022), https://doi.org/10.1002/adma.202200756.
[28] X. Li, C. Wang, J. Yang, Y. Xu, Y. Yang, J. Yu, J.J. Delgado, N. Martsinovich, X. Sun, X.S. Zheng, W. Huang, J. Tang, PdCu nanoalloy decorated photocatalysts for efficient and selective oxidative coupling of methane in flow reactors, Nat. Commun 14 (2023), https://doi.org/10.1038/s41467-023-41996-y.
[29] X. Li, C. Li, Y. Xu, Q. Liu, M. Bahri, L. Zhang, N.D. Browning, A.J. Cowan, J. Tang, Efficient hole abstraction for highly selective oxidative coupling of methane by Au-sputtered TiO2 photocatalysts, Nat. Energy 8 (2023) 1013–1022, https://doi.org/10.1038/s41560-023-01317-5.
[30] T. Schultz, T. Lenz, N. Kotadiya, G. Heimel, G. Glasser, R. Berger, P.W.M. Blom, P. Amsalem, D.M. de Leeuw, N. Koch, Reliable Work Function Determination of Multicomponent Surfaces and Interfaces: The Role of Electrostatic Potentials in Ultraviolet Photoelectron Spectroscopy, Adv. Mater. Interfaces 4 (2017), https://doi.org/10.1002/admi.201700324.
[31] Y. Liu, M. Zhang, Z. Wang, J. He, J. Zhang, S. Ye, X. Wang, D. Li, H. Yin, Q. Zhu, H. Jing, Y. Weng, F. Pan, R. Chen, C. Li, F. Fan, Bipolar charge collecting structure enables overall water splitting on ferroelectric photocatalysts, Nat. Commun 13 (2022) 4245, https://doi.org/10.1038/s41467-022-32002-y.
[32] U. Diebold, The surface science of titanium dioxide, Surf. Sci. Rep 48 (2003) 53–229, https://doi.org/10.1016/S0167-5729(02)00100-0.
[33] E. Farfan-Arribas, R.J. Madix, Role of Defects in the Adsorption of Aliphatic Alcohols on the TiO $_2$ (110) Surface, J. Phys. Chem. B 106 (2002) 10680–10692, https://doi.org/10.1021/jp020729p.
[34] Z. Zhang, O. Bondarchuk, J.M. White, B.D. Kay, Z. Dohnálek, Imaging adsorbate O-H bond cleavage: Methanol on TiO2(110), J. Am. Chem. Soc 128 (2006) 4198–4199, https://doi.org/10.1021/ja058466a.
[35] Q. Guo, C. Xu, Z. Ren, W. Yang, Z. Ma, D. Dai, H. Fan, T.K. Minton, X. Yang, Stepwise photocatalytic dissociation of methanol and water on TiO 2(110), J. Am. Chem. Soc 134 (2012) 13366–13373, https://doi.org/10.1021/ja304049x.
[36] K.R. Phillips, S.C. Jensen, M. Baron, S.C. Li, C.M. Friend, Sequential photo-oxidation of methanol to methyl formate on TiO 2(110), J. Am. Chem. Soc 135 (2013) 574–577, https://doi.org/10.1021/ja3106797.